Published in final edited form as:
Transl Stroke Res. 2013 October ; 4(5): 500–506. doi:10.1007/s12975-013-0285-y.

Dynamic Contrast-Enhanced MRI Evaluation of Cerebral Cavernous Malformations

B. L. Hart,
Department of Radiology, University of New Mexico, MSC10 5530, 1, Albuquerque, NM 87131-0001, USA

S. Taheri,
Department of Radiology, Medical University of South Carolina, Bioengineering Bldg- 68 President St., MSC 323, RM 206, Charleston, SC 29425, USA

G. A. Rosenberg, and
Department of Neurology, University of New Mexico, MSC10 5620, 1, Albuquerque, NM 87131-0001, USA

L. A. Morrison
Department of Neurology, University of New Mexico, MSC10 5620, 1, Albuquerque, NM 87131-0001, USA

B. L. Hart: bhart@salud.unm.edu; S. Taheri: taheri@musc.edu; G. A. Rosenberg: GRosenberg@salud.unm.edu; L. A. Morrison: LMorrison@salud.unm.edu

Abstract

The aim of this study is to quantitatively evaluate the behavior of CNS cavernous malformations (CCMs) using a dynamic contrast-enhanced MRI (DCEMRI) technique sensitive for slow transfer rates of gadolinium. The prospective study was approved by the institutional review board and was HIPPA compliant. Written informed consent was obtained from 14 subjects with familial CCMs (4 men and 10 women, ages 22–76 years, mean 48.1 years). Following routine anatomic MRI of the brain, DCEMRI was performed for six slices, using T1 mapping with partial inversion recovery (TAPIR) to calculate T1 values, following administration of 0.025 mmol/kg gadolinium DTPA. The transfer rate (Ki) was calculated using the Patlak model, and Ki within CCMs was compared to normal-appearing white matter as well as to 17 normal control subjects previously studied. All subjects had typical MRI appearance of CCMs. Thirty-nine CCMs were studied using DCEMRI. Ki was low or normal in 12 lesions and elevated from 1.4 to 12 times higher than background in the remaining 27 lesions. Ki ranged from 2.1E–6 to 9.63E–4 min^{-1}, mean 3.55E–4. Normal-appearing white matter in the CCM patients had a mean Ki of 1.57E–4, not statistically different from mean WM Ki of 1.47E–4 in controls. TAPIR-based DCEMRI technique permits quantifiable assessment of CCMs in vivo and reveals considerable differences not seen with conventional MRI. Potential applications include correlation with biologic behavior such as lesion growth or hemorrage, and measurement of drug effects.

Conflict of Interest Blaine L. Hart, MD and Saeid Taheri, Ph.D. declares that they have no conflict of interest. Leslie A. Morrison, MD declares that she has received travel/accommodations meeting expenses from the Association of American Medical Colleges, American Association Neurology, and the CDC. Gary Rosenberg, MD declares that he has received consultancy fees from Novartis Pharmaceuticals.

Compliance with Ethics Requirements All procedures followed were in accordance with the ethical standards of the responsible committee on human experimentation (institutional and national) and with the Helsinki Declaration of 1975, as revised in 2008 [5]. Informed consent was obtained from all patients for being included in the study.

Keywords

MRI dynamic contrast enhanced; Brain/brain stem; Genetic defects

Introduction

Cerebral or CNS cavernous malformations (CCMs) are readily diagnosed by MRI, but their clinical course is characteristically unpredictable, ranging from benign to catastrophic [1–5] CCMs occur in both familial and sporadic forms, with an estimated overall prevalence of 0.5–1 % in the general population [6, 7]. Mutations in three confirmed genes are known to cause human CCMs, supported by a variety of tissue and animal studies demonstrating abnormal vascular permeability and an abnormal blood–brain barrier in CCMs [8–12]. Although blood flow within CCMs is slow, intra-and extra-lesional hemorrhage is common, leading to growth of lesions or acute neurological changes. De novo CCMs appear over time in familial cases and can number into the hundreds. Epilepsy, headaches, focal neurological deficits, and even death can occur, but up to 50 % of patients remain asymptomatic.

Despite the clinical risks associated with CCMs, treatment options are limited, especially for patients with multiple CCMs. Surgical resection and focused radiation can be performed, but the risk-benefit ratio of these treatments is unclear, absent our ability to predict the risk of hemorrhage in individual lesions. Although no medical therapy for CCMs has been shown effective in humans, animal models show prevention of CCM formation with statins [12], fasudil [13], and sorafenib [14]. Unfortunately, the relatively low hemorrhage rate of individual CCMs means that a therapeutic trial would involve large numbers of patients over many years.

These obstacles to medical treatment could be reduced by an in vivo test that (a) demonstrates differences in physiology of individual lesions that predict hemorrhage or growth and (b) provides a quantitative tool that could serve as a surrogate treatment endpoint. Dynamic contrast-enhanced MRI (DCEMRI) is especially promising because a variety of laboratory, animal, and ultrastructural techniques all point to a role of abnormal capillary permeability in the formation of CCMs, and permeability is part of what can be measured by DCEMRI. Many previous studies of DCEMRI have evaluated alterations of permeability, either in tumors, within which neovascularity may accompany active proliferation, or in stroke. Vascular malformations, specifically CCMs, are an additional disease category in which permeability may play a crucial role; however, CCMs differ in that permeability, although abnormal, is still much less than that seen in tumors or markedly ischemic tissue. An inversion–recovery-based technique, which permits T1 calculation, can measure the low transfer rate (Ki) in normal brain tissue as well as in pathologic conditions. The purpose of this study was to evaluate the quantitative behavior of CCMs using a DCEMRI technique sensitive to the slow transfer of gadolinium into the brain.

Materials and Methods

Subjects

This prospective HIPPA-compliant study protocol was approved by the institutional review board, and written informed consent was obtained from all study subjects before the investigation. Sixteen volunteers (5 men and 11 women) with personal and/or family history suggestive of familial CCM were studied. Two were excluded from analysis, one because she had no CCM on MRI, and the other due to excessive motion during the study. Of the 14 familial CCM patients analyzed (4 men and 10 women), mean age was 48.1 years, range 22–76 years.

Control data were available from 17 healthy volunteers (ages 22–75) studied under a previous protocol with the same acquisition parameters and imaging system.

MRI Technique

All studies were performed on a 1.5 T imaging system (Siemens) with a standard eight channel array head coil. MRI sequences included sagittal T1-weighted MPRAGE and axial fast spin echo PD/T2, FLAIR, DWI, and gradient echo T2-weighted sequences, followed by DCEMRI performed using a TAPIR-based method (T1 mapping with partial inversion recovery) to calculate T1 values. TAPIR is based on Look-Locker approach [15] and consists of a magnetization preparation module followed by segmented echo planar imaging readout. To obtain unbiased determination of T1, a version of TAPIR corrected for non-perfect inversion of magnetization (by employing adiabatic fast passage inversion pulse instead of rectangular inversion pulse) was used to obtain a dynamic series of eight T1-weighted image sets [16].

TAPIR was used to obtain a dynamic series of eight T1-weighted image sets, covering six slices selected to cover the largest CCMs for each subject. The first T1 map was acquired preinjection, and the rest were acquired as time series data of MR images after bolus intravenous injection of low-dose gadolinium-DTPA (Gd-DTPA) (0.025 mmol/kg, or 1/4 of usual clinical dose). This dose of gadolinium provided adequate contrast-to-noise and less nonlinearity in T1-(Gd-DTPA) relationship [17, 18] longitudinal relaxation time.

T1 was quantified with a fast TAPIR sequence [19, 20] with the following parameters: TR=15 ms; banded readout scheme with three echoes at 2.8, 5.1, and 7.4 ms; α =25°; FOV= 220 mm×220 mm, slice thickness = either 4.0 or 5.0 mm, number of averages=1, matrix size=128×128, receiver band-width=50 kHz; 20 time-points sampled on the relaxation curve; TI=30 ms and preparation delay=2 s. These parameters produce in-plane resolution of 1.72 mm×1.72 mm, and a sampling interval of 3 min. Imperfections due to the non-perfect inversion of magnetization in TAPIR were corrected as required for an unbiased determination of T1.

Data Analysis

Data processing was performed with custom software written in MATLAB (Mathworks, Natick, MA). Using time series T1 maps representing the change of relaxivity due to Gd-DTPA, the rate of transfer of Gd-DTPA from vascular compartment into tissue compartment, Ki, was calculated by employing a set of ordinary differential equations first proposed by Patlak [21] and used by others [22, 23]. Pixel-by-pixel values for Ki were calculated and color coded to construct permeability maps (Figs. 1 and 2). White matter (WM) and lesion volume were segmented on the basis of FLAIR images and used as masks to generate the mean Ki in both lesions and WM areas.

The R statistical computing environment (R Development Core Team, 2007) was used for statistical analysis. Comparisons of Ki were made for (a) intrasubject Ki between individual CCMs and subject's nonlesional WM at the same level using paired *t* test and (b) intergroup for nonlesional WM of CCM subject and control subject WM using unpaired *t* test.

We examined two possible indicators of the effect of previous hemorrhage as follows: correlation of Ki with the ratio of the diameter of the central core of the CCM to the thickness of the surrounding hemosiderin rim based on T2 images, as a measure of prior peripheral hemorrhage, and correlation of Ki with lesion volume, as a measure of internal hemorrhage within a CCM.

Results

Fourteen patients had MRI findings characteristic of CCMs. Larger CCMs showed discrete reticulated structures containing blood products of varying ages with a peripheral hemosiderin rim. Numerous smaller CCMs were evident on T2-gradient recall sequences. For seven subjects, we analyzed one CCM, and for seven subjects, we were able to analyze from 2–10 CCMs. A total of 39 CCMs were analyzed in the 14 subjects.

DCEMRI revealed considerable heterogeneity of CCMs relative to blood–brain barrier behavior (Figs. 1 and 2). Ki ranged from 2.14E–6 to 9.63E–4 min^{-1}, with a mean of 3.55E–4 (Table 1). Comparison of lesion Ki to nonlesional WM on the same slices was highly significantly different (p <0.0001). The Ki of CCMs compared to control subject WM was also significantly different (p <0.0001). The ratios of lesion Ki compared to nonlesional WM on the same slices ranged from 12 lesions at or below background WM levels to 27 CCMs with ratios from 1.4 to 12 times higher than background WM (Table 1). Larger CCMs also demonstrated heterogeneous patterns in some cases, as illustrated in Fig. 2. Ki did not show clear correlation with visual appearance of CCMs on routine MRI. The Ki of 22 out of 39 lesions was over double that of nearby intrasubject WM.

Size was a factor, in that all but one of the CCMs with normal or low Ki were small (volume <600 mm^3) (Fig. 3); however, 17 out of 27 small CCMs still demonstrated elevated Ki, including the CCM with the highest Ki. One larger CCM with low Ki was very heterogeneous, with areas of both elevated and decreased Ki (Fig. 2); mean Ki for the lesion was close to background. There was a trend toward, but not statistically significant correlation between, lesion volume and Ki. Most of the small lesions had a high ratio of thickness of the hemosiderin rim to the size of the internal core portion of the CCM, and lesions with less hemosiderin rim had higher Ki. The small lesion mentioned above, with the highest Ki, had almost no hemosiderin rim.

Mean Ki of CCM background WM was 1.57E–4 min^{-1} (range 5.39E–5 to 5.66E–4), higher than control mean WM of 1.47E–4, but not statistically significant.

Discussion

Conventional MRI is important for diagnosis and anatomic characterization of CCMs but is limited in evaluation of the biologic behavior of CCMs. Abnormal permeability is known to be a major factor in CCM pathophysiology. Because permeability has a central role in the model of transfer rate utilized, we investigated a DCEMRI method sensitive for slow but abnormal transfer in CCMs.

TAPIR-based DCEMRI, using T1 calculation from a high density of time points, has particular advantages for vascular malformations with slow flow. Typical applications of DCEMRI based on signal intensity measurements are suited to lesions such as tumors with a high rate of leakage through the blood–brain barrier [24, 25]. The transfer rate within CCMs is much slower. The lesions themselves are mostly vascular tissue, neither gray nor white matter, but because most CCMs we evaluated were within WM or at the gray–white junction, we compared to nearby WM Ki. Although longer periods of data acquisition are needed for measuring low transfer rates, T1-based measurement avoids nonlinearity inherent in T2*-based methods, and use of T1 measurements rather than signal intensity changes should reduce specific machine-dependent variability. Sampling several points during the inversion recovery sequence permits calculation of T1 for each pixel.

We found that TAPIR-based DCEMRI reveals abnormal transfer rate of gadolinium in CCMs and shows considerable heterogeneity of lesions. This heterogeneity in lesion

permeability may underlie the variability in lesion biologic behavior, specifically, the likelihood of subsequent hemorrhage. Evaluating a relationship between permeability and hemorrhage will require follow up studies over time.

Until longitudinal data are available, however, the question arises of whether Ki correlates with evidence of previous hemorrhage of CCMs. Determining the extent of previous hemorrhage is complex. For practical purposes, CCMs are visible by MRI because of blood. Some may be intravascular, within the malformation, but we know from pathological studies that there is frequent bleeding, even if only oozing, within malformations. The hemosiderin rim is a presumptive evidence of blood breakdown products being taken up at the periphery of the CCM by macrophages. As far as this type of evidence of prior hemorrhage, there is a general trend for an inverse relationship between Ki and thickness of the hemosiderin rim. However, caution is necessary in interpreting the significance of this finding. Many of these CCMs are smaller lesions. There are several possible reasons that Ki may be lower as follows: (1) With small lesions, volume averaging is an issue and may decrease Ki. (2) Prior hemorrhage and hemosiderin deposition might result in scarring around the CCM, with decreased blood flow and lower Ki in brain around the CCM. (3) Perhaps most importantly, the presence of iron in the hemosiderin may decrease signal detection and artifactually decrease Ki. A thicker hemosiderin rim may for a variety of reasons decrease Ki around the lesion without necessarily reflecting internal permeability. Very small CCMs are below the resolution of this technique.

Another hypothesis relating permeability to CCM characteristics would be that more permeability defects, resulting in higher Ki, may correlate with more intralesional hemorrhage and, therefore, subsequent growth. It is suggestive that among the larger CCMs, Ki ranged from mildly elevated to more than ten times the background rate.

Measured Ki of nonlesional WM, without obvious CCMs on gradient recall MRI, is close to that of control WM but does show variability. Factors possibly contributing to heterogeneous Ki in WM include presence of very small CCMs that might increase permeability, signal loss from small amounts of hemosiderin, contribution from a very leaky nearby CCM, and the possibility of a more diffuse permeability defect in capillaries throughout the brain. Because of this variability, we evaluated both calculated Ki and Ki ratios.

We are especially interested in the potential for DCEMRI to provide a quantitative tool for evaluating the effects of drugs on CCMs. Despite intriguing animal studies, no drugs have as yet proven effective and safe for this purpose in humans. Human studies ultimately need to show a decreased rate of hemorrhage and/or new lesion formation, but such studies could be very expensive and time consuming. For example, a 5-year outcome study for a hypothetical drug with relative risk of 0.80 of reducing recurrent intracranial hemorrhage or nonhemorrhagic focal neurological deficit over 5 years of follow-up, with a significance level of 5 % and power of 80 %, would require 1,150 patients (personal communication, R. Al-Shahi Salman). Higher power requirements or less drug effect would require even larger numbers of patients. A surrogate marker of biologic activity of a drug on permeability within CCMs could be very important in identifying the best candidates for such trials. DCEMRI can be performed in animals and could also be a bridge in human studies for evaluating therapeutic effects prior to large-scale trials.

Limitations of this technique include the acquisition time for the TAPIR sequence (approximately 24 min), which makes patient motion challenging, and the complex postprocessing. The latter will likely decrease with technical and software improvements. No pathological correlation was available in this in vivo human study. The model also has

inherent limitations. Ki, modeled as the product of permeability, surface area, and tissue density, should not be assumed to be an actual measure of permeability. Tissue density is likely similar for CCMs and brain (unless there is calcification), but surface area within CCMs is likely to be different from normal brain tissue. Nevertheless, permeability is clearly a large factor in Ki. The greatest advantage is the quantitative repeatable nature of the test.

TAPIR-based DCEMRI offers a physiological tool for evaluation of CCMs that can reveal differences among lesions that otherwise appear similar on routine MRI, potentially correlating with clinical outcomes, and provides a quantifiable measurement for assessment of drug effects on permeability.

Acknowledgments

This project was supported in part by NIH grant U54 NS065705 as well the National Center for Research Resources and the National Center for Advancing Translational Sciences of the National Institutes of Health through Grant Number UL1 TR000041. The content is solely the responsibility of the authors and does not necessarily represent the official views of the NIH. This project was supported in part by the Dedicated Health Research Funds of the University of New Mexico School Of Medicine.

References

1. Aiba T, Tanaka R, Koike T, Kameyama S, Takeda N, Komata T. Natural history of intracranial cavernous malformations. J Neurosurg. 1995; 83:56–9. [PubMed: 7782850]
2. Al-Shahi Salman RA, Hall JM, Horne MA, et al. Untreated clinical course of cerebral cavernous malformations: a prospective population-based cohort study. Lancet. 2012; 11:217–24.
3. Zambramski JM, Wascher TM, Spetzler RF, et al. The natural history of familial cavernous malformations: results of an ongoing study. J Neurosurg. 1994; 80:422–32. [PubMed: 8113854]
4. Labauge P, Brunereau L, Laberge S, Houtteville JP. Prospective follow-up of 33 asymptomatic patients with familial cerebral cavernous malformations. Neurology. 2001; 57:1825–8. [PubMed: 11723271]
5. Flemming KD. Predicting the clinical behaviour of cavernous malformations. Lancet. 2012; 11:202–3.
6. Robinson JR, Awad IA, Little JR. Natural history of cavernous angioma. J Neurosurg. 1991; 75:709–14. [PubMed: 1919692]
7. Leblanc GG, Golanov E, Award IA, Young WL. Biology of vascular malformations of the brain. Stroke. 2009; 40:694–702.
8. Schneider H, Errede M, Ulrich NH, Virgintino D, Frei K, Bertalanffy H. Impairment of tight junctions and glucose transport in endothelial cells of human cerebral cavernous malformations. J Neuropathol Exp Neurol. 2011; 70:417–29. [PubMed: 21572340]
9. Tu J, Stoodley MA, Morgan MK, Storer KP. Ultrastructural characteristics of hemorrhagic, nonhemorrhagic, and recurrent cavernous malformations. J Neurosurg. 2005; 103:903–9. [PubMed: 16304995]
10. Clatterbuck RE, Eberhart CG, Crain BJ, Rigamonti D. Ultrastructural and immunocytochemical evidence that an incompetent blood–brain barrier is related to the pathophysiology of cavernous malformations. J Neurol Neurosurg Psychiatry. 2001; 71:188–92. [PubMed: 11459890]
11. Kleaveland B, Zheng X, Liu JJ, et al. Regulation of cardiovascular development and integrity by the heart of glass-cerebral cavernous malformation protein pathway. Nat Med. 2009; 15:169–76. [PubMed: 19151727]
12. Whitehead KJ, Chan AC, Navankasattusas S, et al. The cerebral cavernous malformation signaling pathway promotes vascular integrity via Rho GTPases. Nat Med. 2009; 15:177–84. [PubMed: 19151728]
13. McDonald DA, Shi C, Shenkar R, et al. Fasudil decreases lesion burden in a murine model of cerebral cavernous malformation disease. Stroke. 2012; 43:571–4. [PubMed: 22034008]

14. Wüstehube J, Bartol A, Liebler SS, et al. Cerebral cavernous malformation protein CCMI1 inhibits sprouting angiogenesis by activating DELTA-NOTCH signaling. Natl Acad Sci U S A. 2010; 107:12640–5.
15. Look DC, Locker DR. Time saving in measurement of NMR and EPR relaxation times. Rev Sci Instrum. 1969; 41(2)
16. Zaitsev M, Steinhoff S, Shah NJ. Error reduction and parameter optimization of the TAPIR method for fast T1 mapping. Magn Reson Med. 2003; 49(6):1121–32.10.1002/mrm.10478 [PubMed: 12768591]
17. Taheri S, Gasparovic C, Shah NJ, Rosenberg GA. Quantitative measurement of blood–brain barrier permeability in human using dynamic contrast-enhanced MRI with fast T1 mapping. Magn Reson Med. 2011; 65:1036–42. [PubMed: 21413067]
18. Taheri S, Gasparovic C, Huisa BN, et al. Blood–brain barrier permeability abnormalities in vascular cognitive impairment. Stroke. 2011; 42:2158–63. [PubMed: 21719768]
19. Shah NJ, Zaitsev M, Steinhoff S, Zilles K. A new method for fast multislice T(1) mapping. NeuroImage. 2001; 14:1175–85. [PubMed: 11697949]
20. Neeb H, Zilles K, Shah NJ. A new method for fast quantitative mapping of absolute water content in vivo. NeuroImage. 2006; 31:1156–68. [PubMed: 16650780]
21. Patlak CS, Blasberg RG. Graphical evaluation of blood-to-brain transfer constants from multiple-time uptake data. Generalizations. J Cereb Blood Flow Metab. 1985; 5:584–90. [PubMed: 4055928]
22. Ewing JR, Knight RA, Nagaraja TN, et al. Patlak plots of Gd-DTPA MRI data yield blood–brain transfer constants concordant with those of 14C-sucrose in areas of blood–brain opening. Magn Reson Med. 2003; 50:283–92. [PubMed: 12876704]
23. Larsson HB, Courivaud F, Rostrup E, Hansen AE. Measurement of brain perfusion, blood volume, and blood–brain barrier permeability, using dynamic contrast-enhanced T(1)-weighted MRI at 3 T. Magn Reson Med. 2009; 62:1270–81. [PubMed: 19780145]
24. Law M. Advanced imaging techniques in brain tumors. Cancer Imaging. 2009; 9:S4–9. [PubMed: 19965287]
25. Provenzale JM, Wang GR, Brenner T, Petrella JR, Sorensen AG. Comparison of permeability in high-grade and low-grade brain tumors using dynamic susceptibility contrast MR imaging. AJR Am J Roentgenol. 2002; 178:711–6. [PubMed: 11856703]

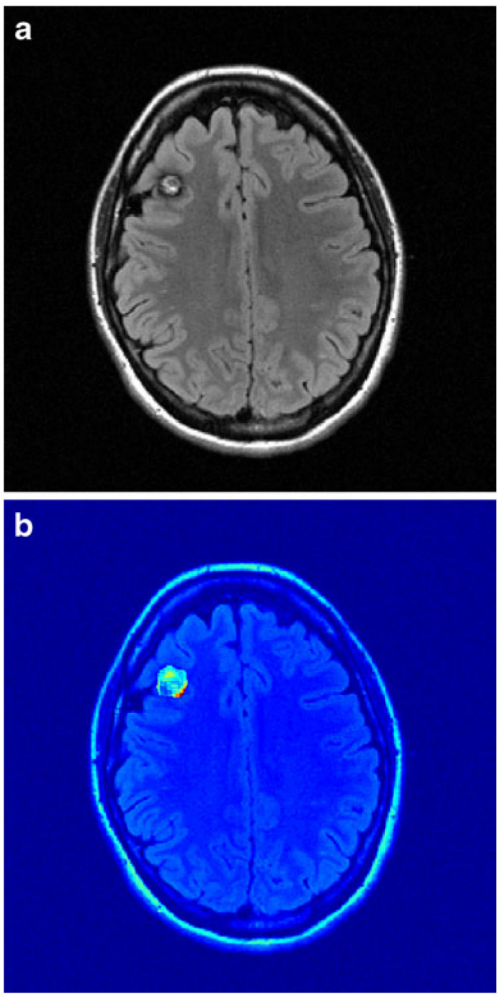

Fig. 1.

Example of CCM and transfer rate map. **a** Axial T2 FLAIR MRI of a subject with familial CCMs shows a right frontal CCM. **b** Ki map shows elevated but heterogeneous Ki within the CCM. Ki of the CCM was 6.84 E–04, and mean Ki of white matter was 1.08 E–04

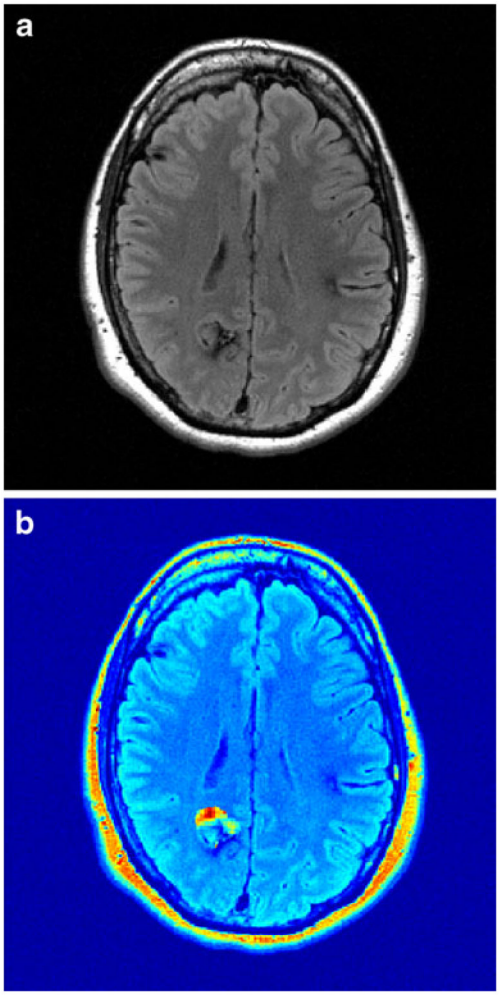

Fig. 2.

Heterogeneous nature of CCM. **a** Axial T2 FLAIR shows a posterior right CCM, as well as small areas of hemosiderin associated with smaller frontal CCMs. **b** Ki map demonstrates that the anterior portion of the right lesion has elevated Ki and the posterior portion has a low Ki; the mean Ki for the lesion is near background

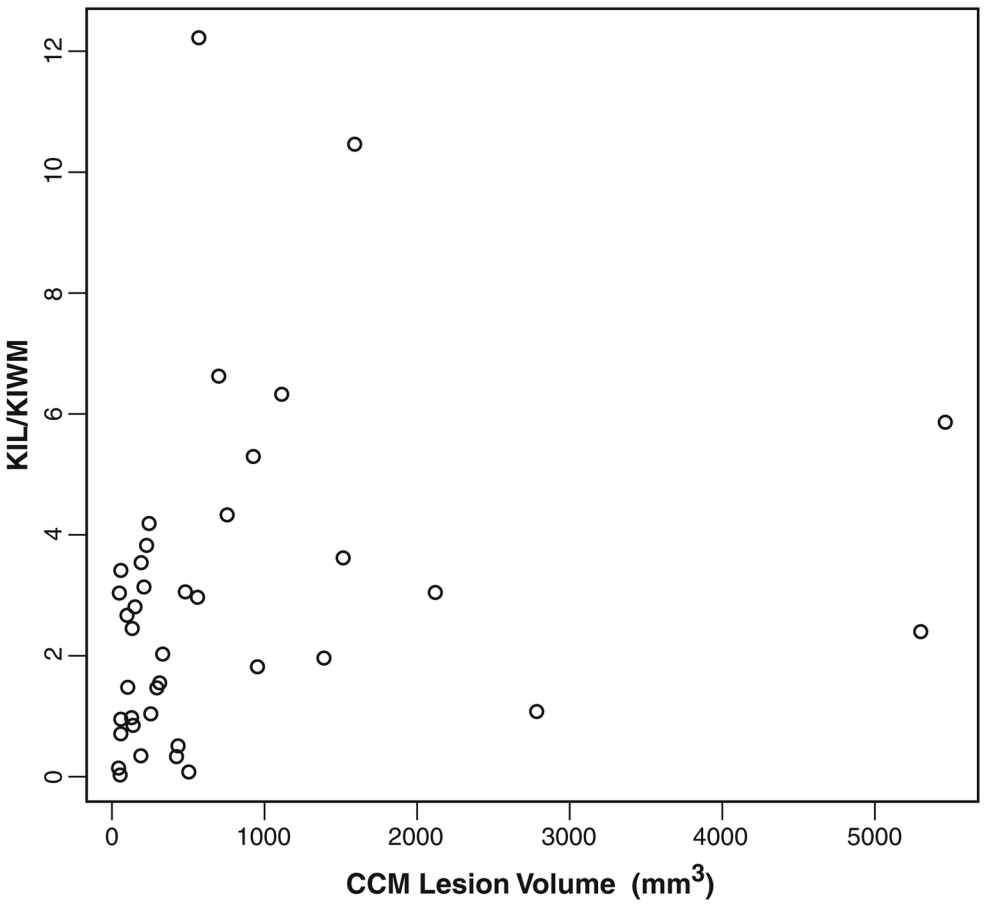

Fig. 3.
Relationship of volume of CCMs (in mm^3) to Ki ratio (CCM/nonlesional WM). Neither loess function nor a linear model fitted to the data showed statistical significance

Table 1

Subject data and CCM Ki analysis

Subject	Sex	Age	Lesion	Ki lesion (min^{-1})	Ki WM	Ratio	Volume mm^3
				E-04	E-04		
1	F	27	1A	3.23	0.61	5.30	925
2	F	22	2A	6.84	1.08	6.33	1,110
3	F	43	3A	0.79	1.16	0.68	57
			3B	0.02	1.11	0.02	56
4	F	39	4A	0.98	3.39	0.29	438
6	F	60	6A	0.26	0.83	0.31	191
7	M	51	7A	3.40	3.22	1.06	2,794
			7B	0.19	3.33	0.06	506
			7C	6.00	3.33	1.80	954
			7D	8.56	2.74	3.12	212
8	F	27	8A	9.63	0.79	12.25	564
9	M	76	9A	2.81	0.92	3.05	486
10	F	61	10A	5.63	0.54	10.45	1,590
			10B	0.54	0.56	0.96	127
			10C	0.81	0.56	1.46	102
			10D	1.46	0.61	2.41	5,323
			10E	2.96	0.68	4.33	747
12	M	36	12A	0.11	1.03	0.10	51
			12B	6.57	1.57	4.18	246
			12C	5.12	1.51	3.39	60
			12D	2.55	5.66	0.45	442
13	F	68	13A	3.26	1.10	2.96	561
			13B	4.45	1.46	3.05	2,124
			13C	2.67	1.40	1.90	1,390
			13D	1.38	0.96	1.44	297
			13E	2.66	0.96	2.78	148
			13 F	6.53	1.85	3.53	189

Transl Stroke Res. Author manuscript; available in PMC 2014 October 01.